Available online at www.sciencedirect.com
ScienceDirect
Colloids and Surfaces A: Physicochem. Eng. Aspects 301 (2007) 271–280
COLLOIDS AND SURFACES A
www.elsevier.com/locate/colsurfa

Theoretical modelling of electrokinetic flow in microchannel networks

Claudio L.A. Berli [a,b,*]

[a] INTEC (UNL-CONICET), Güemes 3450, 3000, Santa Fe, Argentina
[b] Departamento de Física, Facultad de Bioquímica y Ciencias Biológicas, UNL, El Pozo, 3000, Santa Fe, Argentina

Received 15 May 2006; received in revised form 18 December 2006; accepted 19 December 2006
Available online 3 January 2007

Abstract

This work deals with the description of electrokinetic flow in microfluidic networks involving multiple channels intersections. A generalized one-dimensional modelling is carried out to predict flow rate and electric current in each branch of the network, as a function of applied electric potentials and pressure gradients. Mathematical derivations ground on thermodynamic formalisms for electrokinetic phenomena, and takes into account the characteristics of every channel and circulating fluid in the system. The coefficients that relate driving forces and conjugated flows are derived for both slit and cylindrical microchannels, with arbitrary values of surface potential and electric double layer thickness. Calculations are used to rationalize typical operations performed in analytical devices that consist of well-defined microchannel networks. The modelling suggested also provides an accurate basis to study fundamental aspects of electrokinetic phenomena in microfluidic systems.

Keywords: Electrokinetic flow; Microchannel networks; Microfluidics; Analytical devices

1. Introduction

Analytical microfluidic devices, as those currently used in chemical, biological and medical applications, basically consist of different networks of microchannels that connect chambers and reservoirs [1–5]. The architecture of these networks may be more or less complex, involving the basic units drawn schematically in Fig. 1. In order to manipulate the transport of fluids, microchannels are generally subjected to pressure gradients, electric fields, or a combination of the two. Therefore, in view of technological applications, reliable models are necessary to describe the coupled flows of matter and electricity developed in every branch of the network. For this purpose, a sound understanding of the mechanisms governing electrokinetic phenomena in microfluidic systems is required [12].

Detailed treatments of microchannel networks involve the modelling of electrokinetic and transport phenomena in the whole system, considering effects in two and three dimensions, which demands important computational efforts [7,9,12–14]. Nevertheless, if microchannels are sufficiently slim, flows are fully developed and two-dimensional effects are present near the channel intersections only (Reynolds numbers are normally lower than 1 in microchannels [15]). Under these circumstances, one-dimensional modelling applies as a first approximation. This approach greatly simplifies calculations and still provides valuable information to design and operate integrated microfluidic systems. Thus, compact models have been derived by emulating electrical circuits [6,9,16,17]. Although useful in practical manipulations, these models are limited to micro-scale channels and relatively high ionic concentrations, as calculations assume negligibly thin electric double layers (EDL) in relation to channel cross-sectional size. The effect of heterogeneities in channel characteristics is also underestimated. Addressing these issues, a more complete analysis has been proposed to model single junction networks of cylindrical capillaries [8]. However, for the particular case of electro-osmotic flow (EOF), equations reported apply for channel ends exposed to atmospheric pressure only.

It should be observed that the simultaneous presence of both electric potential and pressure gradients need to be considered, because these conjugated forces can rarely be decoupled. In systems driven solely by pressure, streaming phenomena occur when microchannels contain interfacial charge, and hence the electrokinetic ζ-potential is present (see, for instance [18]). Conversely, in systems driven by EOF, pressure differences take place if the ζ-potential varies from one branch to another

* Tel.: +54 342 4559174/75/76/77; fax: +54 342 4550944.
E-mail address: cberli@ceride.gov.ar.

0927-7757/$ – see front matter © 2007 Elsevier B.V. All rights reserved.
doi:10.1016/j.colsurfa.2006.12.066

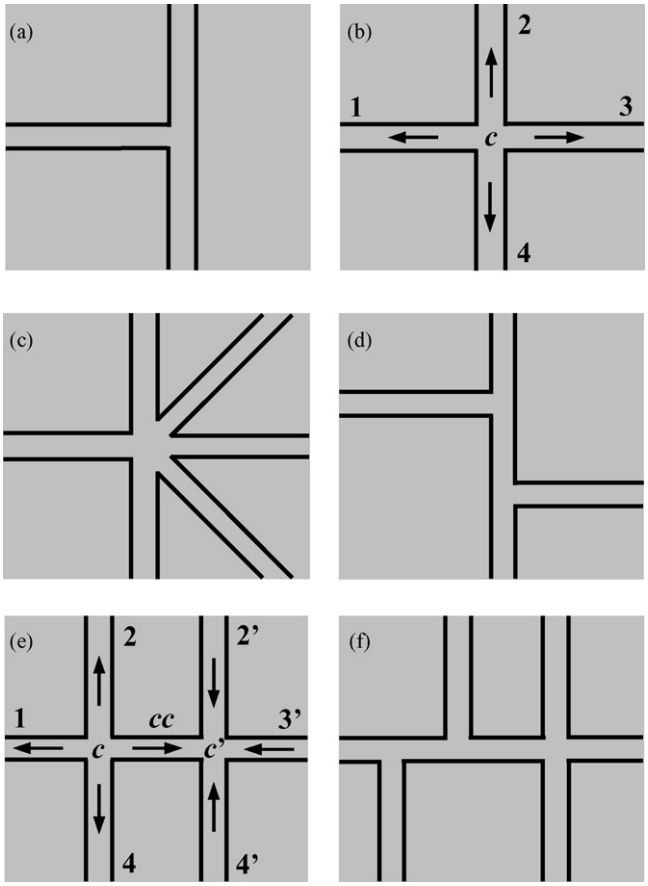

Fig. 1. Schematic representation of different microchannel networks: (a) T-shaped [6], (b) cross-shaped [7], (c) multi-branch [8], (d) double-T [9], (e) double-cross [10], and (f) multi-junction [11]. References cited above are some of several examples found in the recent literature. In particular, schemes (b) and (e) include the nomenclature used here to identify branches and junctions in calculations. Also in these schemes, arrows indicate the positive direction of the flow.

[13,19,20]. Further, even when channel ends are open to atmosphere, pressure gradients arise due to differential meniscus curvatures generated in the reservoirs located at channel ends [21,22], or due to unequal fluid heights, for example, when the plate containing the network is not placed normal to gravity [21,23]. As a last point, it is worth noting that novel applications combine EOF and pressure-driven flow in the same device [24].

In this context of analysis, the present work discusses a generalized modelling of the one-dimensional, steady state, electrokinetic flow in microchannel networks. Systems containing multiple junctions and channels with different characteristics (geometry, surface properties, circulating fluid) are taken into consideration. Calculations are aimed to assess the flows of matter and electricity in each branch of the network, as a function of applied electric potentials and pressure gradients. The modelling is performed in the framework of Onsager relations for electrokinetic phenomena [25]. In this sense, the work deals with a particular, extended application of the general formalism revised in [26] and, more specifically, in [27]. In fact, here the coefficients entering the conductance matrix, which relates driving forces and conjugated flows, are derived for both axial and plane-symmetric electrokinetic flows, with arbitrary values of ζ-potential and EDL thickness. In addition, these results are then used to interpret typical operations carried out in well-defined microfluidic networks.

The paper is organized as follows: in Section 2, the equations required to predict the flow rate and the electric current in networks of microchannels are outlined. These equations include coupling coefficients that must be deduced from the governing equations of electrokinetic flow. For the purposes, theoretical concepts are overviewed in Section 3. Then in Section 4, the coefficients are derived in a general form that involves cylindrical and slit microchannels. In particular, analytic expressions are given for symmetric electrolyte solutions flowing through slit channels with relatively low surface potentials (Appendix A). Finally, in Section 5, some examples are considered to illustrate the capability of the approach to explain situations of practical interest.

2. Conjugated flows in microchannel networks

2.1. Single microchannels

The aim of this section is to quantify the flow rate Q and the electric current I developed in straight microchannels, which contain interfacial charge and the associated EDL of ions in solution. The driving forces are electric potential and pressure differences between the ends of the channels, ΔV and ΔP, respectively. In steady state and isothermal conditions, the simultaneous flows are described by Onsager relations [25]:

$$Q = L_{11}\Delta P + L_{12}\Delta V, \tag{1}$$

$$I = L_{21}\Delta P + L_{22}\Delta V, \tag{2}$$

where L_{11}, L_{12}, L_{21}, and L_{22} are coupling coefficients that depend on the characteristics of both microchannel and fluid, as it will be described in detail in Sections 3 and 4. In particular, the matrix of coefficients is symmetric, i.e., $L_{12} = L_{21}$, thus satisfying Onsager fundamental theorem [25–27]. Eqs. (1) and (2) assume that there are no concentration gradients in the axial direction, which is a good approximation provided the channels are sufficiently slim. When osmotic effects are important, an additional term is involved in these equations [26–28].

2.2. Single junction networks

Given networks with one channel intersection, like those shown in Fig. 1a–c, it is of interest to predict the flow rate and the electric current in every branch. For this purpose, the following conservation equations are written:

$$\sum_{i=1}^{N} Q_i = 0, \tag{3}$$

$$\sum_{i=1}^{N} I_i = 0, \tag{4}$$

where sub index i refers to branch number and N is the total number of branches in the network (for example, $N = 4$ in Fig. 1b). Eq. (3) derives from a simple mass balance for incompressible

fluids with uniform density throughout the network. Eq. (4), also known as Kirchoff law for circuit nodes, establishes the electric charge conservation. Introducing Eqs. (1) and (2) for each branch, Eqs. (3) and (4) result,

$$\sum_{i=1}^{N} L_{11,i}\Delta P_i + L_{12,i}\Delta V_i = 0, \tag{5}$$

$$\sum_{i=1}^{N} L_{21,i}\Delta P_i + L_{22,i}\Delta V_i = 0, \tag{6}$$

with the following definitions: $\Delta P_i = P_i - P_c$ and $\Delta V_i = V_i - V_c$. Here, P_i and V_i are, respectively, pressures and potentials applied to the end of the ith branch, while P_c and V_c are the values reached at the junction c. As indicated in Fig. 1b, flows are positive going out of the junction.

In well-characterized networks, P_c and V_c are the only unknowns. These independent variables can be determined by solving the system of linear equations given by (5) and (6), which is rearranged in a form suitable for the application of Cramer rule:

$$\begin{bmatrix} \sum_{i=1}^{N} L_{11,i} & \sum_{i=1}^{N} L_{12,i} \\ \sum_{i=1}^{N} L_{21,i} & \sum_{i=1}^{N} L_{22,i} \end{bmatrix} \begin{bmatrix} P_c \\ V_c \end{bmatrix} = \begin{bmatrix} \sum_{i=1}^{N} L_{11,i} P_i + L_{12,i} V_i \\ \sum_{i=1}^{N} L_{21,i} P_i + L_{22,i} V_i \end{bmatrix}, \tag{7}$$

or equivalently, $\mathbf{A}\cdot\mathbf{z} = \mathbf{a}$, where $\mathbf{A}$ is the (2×2) matrix of coefficients, $\mathbf{z}$ the vector containing the variables ($z_1 = P_c$, $z_2 = V_c$), and $\mathbf{a}$ is the vector that consists of the summations on the right hand side (RHS) of Eq. (7). Therefore, provided det $\mathbf{A}$ is not zero, the unknowns are calculated as $z_r = \det \mathbf{A}_r / \det \mathbf{A}$, where $\mathbf{A}_r$ consists of matrix $\mathbf{A}$ with the rth column replaced by vector $\mathbf{a}$. Once P_c and V_c are determined, the flow rate and electric current are obtained from Eqs. (1) and (2), respectively, for any branch of the network.

2.3. Double junction networks

For networks with a second junction c' and the associated branches i' (Fig. 1e), the following balances need to be considered, apart from Eqs. (3) and (4):

$$\sum_{i'=1'}^{N'} Q_{i'} = 0, \tag{8}$$

$$\sum_{i'=1'}^{N'} I_{i'} = 0, \tag{9}$$

where N' is the number of branches of the second junction. In agreement with the sign convention defined in Fig. 1e, pressure and potential differences related to c' are $\Delta P_{i'} = P_{c'} - P_{i'}$ and $\Delta V_{i'} = V_{c'} - V_{i'}$, respectively. In addition, the branch that connects the junctions is designated cc (common channel), thus $\Delta P_{cc} = P_{c'} - P_c$ and $\Delta V_{cc} = V_{c'} - V_c$. In order to find the 4 unknowns involved in this problem, i.e., P_c, V_c, $P_{c'}$ and $V_{c'}$, the system of equations composed by (3), (4), (8) and (9) is expressed,

$$\begin{bmatrix} \sum_{i=1}^{N} L_{11,i} & \sum_{i=1}^{N} L_{12,i} & -L_{11,cc} & -L_{12,cc} \\ \sum_{i=1}^{N} L_{21,i} & \sum_{i=1}^{N} L_{22,i} & -L_{21,cc} & -L_{22,cc} \\ -L_{11,cc} & -L_{12,cc} & \sum_{i'=1'}^{N'} L_{11,i'} & \sum_{i'=1'}^{N'} L_{12,i'} \\ -L_{21,cc} & -L_{22,cc} & \sum_{i'=1'}^{N'} L_{21,i'} & \sum_{i'=1'}^{N'} L_{22,i'} \end{bmatrix} \times \begin{bmatrix} P_c \\ V_c \\ P_{c'} \\ V_{c'} \end{bmatrix} \begin{bmatrix} \sum_{i\neq cc}^{N} L_{11,i} P_i + L_{12,i} V_i \\ \sum_{i\neq cc}^{N} L_{21,i} P_i + L_{22,i} V_i \\ \sum_{i'\neq cc}^{N'} L_{11,i'} P_{i'} + L_{12,i'} V_{i'} \\ \sum_{i'\neq cc}^{N'} L_{21,i'} P_{i'} + L_{22,i'} V_{i'} \end{bmatrix}. \tag{10}$$

By analogy with the treatment given above to the single junction problem, the vectorial form of Eq. (10) is $\mathbf{B}\cdot\mathbf{z} = \mathbf{b}$, where $\mathbf{B}$ is the (4×4) matrix of coefficients, $\mathbf{z}$ the vector of the unknowns ($z_1 = P_c$, $z_2 = V_c$, $z_3 = P_{c'}$, $z_4 = V_{c'}$), and $\mathbf{b}$ is the vector on the RHS of Eq. (10). As before, the pressures and potentials in the junctions are $z_r = \det \mathbf{B}_r / \det \mathbf{B}$, where $\mathbf{B}_r$ consists of matrix $\mathbf{B}$ with the rth column replaced by vector $\mathbf{b}$.

2.4. Further considerations

It may be readily inferred the way in which this methodology is extended to networks with three or more channel intersections, where the number of unknowns doubles the number of junctions. In the case shown in Fig. 1f, for example, the unknowns are 6 and hence one has to handle 6×6 matrices. In any case, calculations can be carried out by using standard mathematical software. Therefore, if the applied pressures and potentials are given, and the matrix of coefficients is known for the system, the pressures and potentials at the junctions can be calculated, and then both Q and I are obtained for every branch in the network.

The above analysis is general and valid for different channel geometries and electrolyte solutions [27], the characteristics of which enter through the coupling coefficients. Thus, the following task in this modelling consists in finding the expressions of L_{11}, L_{12} and L_{22} from the governing equations of electric and hydrodynamic fields in microchannels.

3. Fundamentals of electrokinetic phenomena

This section accounts for the steady-state electrokinetic flow developed in straight microchannels. For the sake of simplicity, axial and plane-symmetric flows are considered, which match those developed in cylindrical and slit microchannels, respectively (Fig. 2a). The unidirectional flow domain of these geometries is illustrated in a unified form in Fig. 2b, where d is the half-space between the plates in slits, or the inner radius in cylindrical capillaries. Both fluid velocity and electric current are established in the axial direction y, and vary in the transverse direction x.

Previous analysis can be found in several papers considering slits [29–31] and cylindrical capillaries [28,32,33], as well as in wider texts concerning hydrodynamics and interface science [34,35]. More complex geometries require elaborate calcula-

tions (for instance [36]) that are beyond the aim of the present work. A similar comment may be added in relation to time-dependent starting flows [37]. In what follows, the subject is briefly reviewed and the main equations are outlined, in order to derive the expressions of the coupling coefficients afterwards in Section 4.

3.1. Electric field in the fluid domain

The total electric potential involves two contributions: external potentials applied to channel ends, and EDL potentials associated with charged solid–fluid interfaces (Sections 3.2 and 3.3). The electric potential distribution $\phi(x, y)$ is governed by Poisson equation,

$$-\varepsilon\nabla^2\phi(x, y) = \rho_e, \tag{11}$$

where ε is the electric permittivity and $\rho_e = e\sum_k z_k n_k$ is the electric charge density of the electrolyte solution, which is obtained as the summation over all type-k ions, with valence z_k and number density n_k (e is the elementary charge). As mentioned before, if microchannels are slim enough ($l/d \gg 1$; Fig. 2a), the ion densities are quite uniform along the channel, and hence $\partial^2\phi/\partial y^2 \approx 0$. Consequently, the electric field in the axial direction ($-\partial\phi/\partial y$) will be also uniform, and can be readily calculated from the potential difference between the ends of the channel:

$$\frac{\partial\phi}{\partial y} = \frac{\Delta V}{l}. \tag{12}$$

In addition, the distribution of ions will be determined solely by the variation of ϕ in the transverse direction x. For these reasons, the total potential is normally written $\phi(x, y) = \psi(x) + V(y)$, where $\psi(x)$ is the EDL potential at equilibrium state and $V(y)$ is the applied potential [28,33,34].

3.2. Standard model for the fluid–solid interface

Fig. 2c presents a highly schematic representation of the interfacial region of microchannels. The electric potential ψ_s developed at $x = s$, in relation to the reference potential ψ_0 at $x = 0$, depends on the charge generation mechanism of the surface [35]. In principle, it may be thought that solid walls expose towards the fluid a certain number n_s of specific sites able to release or take H^+ ions. Hence, in equilibrium with an aqueous electrolyte solution, the surface becomes electrically charged (in general, negatively) with a surface charge density,

$$q_s = en_s\alpha(\mathrm{pH}), \tag{13}$$

where α(pH) is the pH-dependent, net fraction of ionized sites on the wall [38]. The compact layer ($s \geq x \geq d$; Fig. 2c) is commonly assumed to be free of charges due to the finite size of hydrated ions (specific ion adsorption is not considered here). Thus, the potential drops linearly across this layer to reach the value ψ_d at $x = d$, also designated outer Helmholtz plane [35,39]. In the diffuse layer ($d \geq x \geq 0$; Fig. 2c), the potential decreases in a non-linear form, because of the screening produced by counterions and other electrolyte ions (Section 3.3).

The electroneutrality condition establishes that the surface charge density is balanced with the total charge in the diffuse layer of ions:

$$q_s = -\int_0^d \rho_e(x)\,\mathrm{d}x. \tag{14}$$

Therefore, Eqs. (13) and (14) provide a relationship between the surface potential and the physicochemical characteristics of the solution. In this sense, suitable expressions of α(pH) in terms of dissociation/association constants of surface sites are available [38]. Furthermore, appropriate theoretical descriptions have been recently reported for interfaces containing weak acid groups, such as silanol in fused silica capillaries [40], and carboxyl in synthetic polymer materials [41].

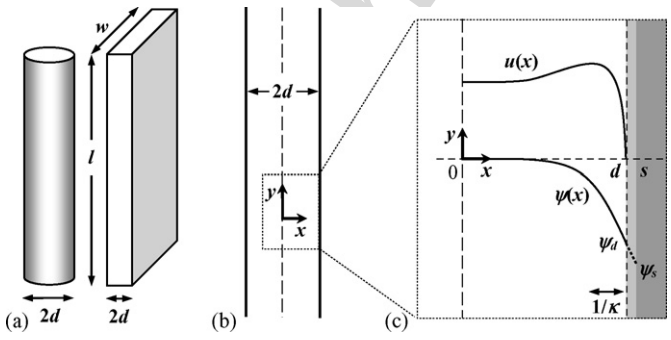

Fig. 2. Schematic representation of: (a) cylindrical and slit microchannels; (b) flow domain and coordinate system used in calculations; (c) solid–liquid interface, involving the EDL potential $\psi(x)$, EDL thickness $1/\kappa$ and velocity profile $u(x)$ (arbitrary drawings).

3.3. Ion and potential distributions in the EDL

In order to find the ion distributions $n_k(x)$ at equilibrium state, the x-component of Nernst–Plank equation is considered [34,35]. Taking into account that there is no radial flux of ions nor flow in the direction x, this equation yields the Boltzmann-type distributions for the kth ionic species in the diffuse layer: $n_k(x) = n_{0,k}\exp[-z_k e(\psi - \psi_0)/k_B T]$, where $n_{0,k} = n_k(0)$ and $\psi_0 = \psi(0)$ are, respectively, ion densities and electric potential at the channel centerline, k_B is the Boltzmann constant, and T is the absolute temperature. With these expressions of $n_k(x)$, and considering the assumptions made above on $\phi(x, y)$, Eq. (11) yields the following relation between EDL potential and ion densities, namely Poisson–Boltzmann equation:

$$\frac{1}{x^m}\frac{\partial}{\partial x}\left(x^m\frac{\partial\psi}{\partial x}\right) = -\frac{e}{\varepsilon}\sum_k z_k n_{0,k}\,\exp\left(-\frac{z_k e(\psi - \psi_0)}{k_B T}\right). \tag{15}$$

In this expression and hereafter, m is used to describe either plane-symmetric ($m = 0$) or axis-symmetric ($m = 1$) geometries [40]. The boundary conditions required to solve Eq. (15) in the flow domain of microchannels are,

$$x = 0, \quad \frac{\partial\psi}{\partial x} = 0; \tag{16}$$

$$x = d, \quad \psi = \psi_d. \tag{17}$$

At this step, it is necessary to introduce the parameter,

$$\kappa = \left(\frac{e^2 \sum_k z_k^2 n_{0,k}}{\varepsilon k_B T} \right)^{1/2}, \tag{18}$$

the inverse of which is the well-known Debye length. For large values of κd (thin EDL in comparison to d; Fig. 2c), the fluid is electrically neutral at the channel centerline ($n_{0,+} = n_{0,-}$) and the reference potential ψ_0 vanishes. This also implies that the concentration of counterions neutralizing the interfacial charge is negligible in comparison with the concentration of electrolyte ions in the bulk, which is usually the case in micro-scale channels at moderate ionic concentrations ($\sim 10^{-3}$ M). Under these conditions, and considering symmetric electrolytes, one obtains the form of Poisson–Boltzmann equation normally used in practice (see (A.1) in the appendix). In contrast, at very low ionic concentrations, or in case of nano-scale channels, where relatively low values of κd are attained, the EDL from opposing surfaces overlap even at low surface potentials. Hence $n_{0,+} \neq n_{0,-}$ and $\psi_0 \neq 0$, which implies special considerations to extract $\psi(x)$ from Eq. (15).

3.4. Fluid velocity and pressure fields

When electric fields are applied along microchannels, electric forces acting on excess ions drag the surrounding liquid, and thus EOF develops. If, in addition, pressure gradients exist in the axial direction, the flow involves a hydrodynamic contribution as well. For Newtonian fluids, the velocity profile $u(x)$ is deduced from the y-component of Navier–Stokes equation [34,35], which provides the momentum balance in the fluid, here written at the steady state:

$$\frac{\partial p}{\partial y} = \mu \frac{1}{x^m} \frac{\partial}{\partial x} \left(x^m \frac{\partial u}{\partial x} \right) + \rho g_y - \rho_e \frac{\partial V}{\partial y}. \tag{19}$$

In this equation, p is the pressure, μ the fluid viscosity, ρ the fluid density, and g_y is the axial component of gravitational acceleration g. Further, $\partial P/\partial y = \partial(p - \rho g_y y)/\partial y$ is defined to be a generalized pressure gradient. In a fully developed flow of incompressible fluids, continuity equation indicates $\partial u/\partial y = 0$, and hence $\partial^2 P/\partial y^2 = 0$ [34,35]. Consequently, the pressure gradient is uniform throughout the channel and can be quantified as,

$$\frac{\partial P}{\partial y} = \frac{\Delta P}{l}. \tag{20}$$

In writing the boundary conditions, one should express that $u(x)$ vanishes at a certain plane parallel to the channel wall, also designated shear plane (see scheme in Fig. 2c), where the value of ψ is identified as the ζ-potential. It is commonly assumed that the shear plane is close to the outer Helmholtz plane, hence $\zeta \approx \psi_d$ [35,39]. Therefore, one may write,

$$x = 0, \qquad \frac{\partial \psi}{\partial x} = 0, \qquad \frac{\partial u}{\partial x} = 0; \tag{21}$$

$$x = d, \qquad \psi = \zeta, \qquad u = 0. \tag{22}$$

With these conditions, and substituting ρ_e from Eq. (15), the solution of Eq. (19) is,

$$u(x) = \frac{(x^2 - d^2)}{2(1+m)\mu} \frac{\partial P}{\partial y} + \frac{\varepsilon [\zeta - \psi(x)]}{\mu} \frac{\partial V}{\partial y}. \tag{23}$$

It is worth to remark that, in this modelling, d is the half-space between the plates in slits ($m = 0$) and the inner radius in cylindrical capillaries ($m = 1$). The first term on the RHS of Eq. (23) accounts for the pressure-driven flow, and the second one represents the EOF.

The potential $\psi(x)$ entering Eq. (23) should be obtained from Eq. (15). Indeed, in the context of the standard electrokinetic model, the EDL is assumed to retain its equilibrium charge distribution even when the electrolyte solution flows [35]. This approximation holds as long as $\Delta V/l$ is small in comparison with $\kappa \zeta_{\psi d}$ and $\kappa k_B T/e$ [27].

3.5. Current density field

Once the velocity field is established, the electric current in the channel is derived from the y-component of Nernst–Plank equation [34,35]. Neglecting axial concentration gradients (because of the assumption of slim microchannels), the flux of kth ionic species is $j_k(x) = n_k u(x) - eFz_k \nu_k n_k \, \partial V/\partial y$, where F is the Faraday constant and ν_k is the ionic mobility. On the RHS of this equation, the first and second terms account for the convective and conductive currents, respectively. The total current density in the flow domain is $j(x) = \sum_k z_k j_k(x)$, i.e.,

$$j(x) = \rho_e u(x) - \sigma \frac{\partial V}{\partial y}, \tag{24}$$

where $\sigma = eF \sum_k z_k^2 \nu_k n_k$ is the electric conductivity of the solution that, as well as ρ_e, depends on transverse direction x through $n_k(x)$.

It should be noted that calculations here neglect the possible conductivity of the stagnant layer [42]. Further, an important effect associated with electric current in microchannels is temperature rising due to internal heat generation, namely Joule effect [12]. In this sense, the present modelling assumes that temperature is constant and uniform throughout the system.

4. Coupling coefficients

The general expressions of flow rate and electric current in uniform, straight channels are, respectively,

$$Q = D_m \frac{1+m}{d^{1+m}} \int_0^d u(x) x^m \, dx, \tag{25}$$

$$I = D_m \frac{1+m}{d^{1+m}} \int_0^d j(x) x^m \, dx, \tag{26}$$

where D_m is the cross-sectional area, being $D_0 = 2wd$ for slits ($m = 0$), and $D_1 = \pi d^2$ for cylindrical channels ($m = 1$). In these expressions, $u(x)$ and $j(x)$ are substituted from Eqs. (23) and (24), which in turn include (12) and (20). Performing integrations and

rearranging, the expressions of Q and I take the respective forms of Eqs. (1) and (2), with the following coefficients:

$$L_{11} = -\frac{D_m d^2}{(1+m)(3+m)\mu l}, \tag{27}$$

$$L_{12} = L_{21} = \frac{D_m \varepsilon \zeta}{\mu l} G_1, \tag{28}$$

$$L_{22} = -\frac{D_m (\varepsilon\zeta/d)^2}{\mu l} G_2 - \frac{D_m \sigma_0}{l} G_3. \tag{29}$$

In fact Eq. (27) is the well-known hydraulic conductance: Eq. (28) represents electro-osmosis/streaming phenomena (Onsager reciprocal relation), and Eq. (29) comprises the electric conductance, where $\sigma_0 = eF\sum_k z_k^2 \nu_k n_{0,k}$ is the conductivity of the electrolyte solution at $x = 0$. The dimensionless geometrical factors appearing in Eqs. (28) and (29) are,

$$G_1 = \frac{1+m}{d^{1+m}} \int_0^d \left(1 - \frac{\psi(x)}{\zeta}\right) x^m \, \mathrm{d}x, \tag{30}$$

$$G_2 = \frac{1+m}{d^{m-1}} \int_0^d \left[\frac{\partial}{\partial x}\left(\frac{\psi(x)}{\zeta}\right)\right]^2 x^m \, \mathrm{d}x, \tag{31}$$

$$G_3 = \frac{1+m}{d^{1+m}} \int_0^d \frac{\sum_k z_k^2 \nu_k n_{0,k} \exp(-z_k e\psi(x)/k_B T)}{\sum_k z_k^2 \nu_k n_{0,k}} x^m \, \mathrm{d}x. \tag{32}$$

It is readily seen that numerical calculations are required to quantify these factors, taking into account that $\psi(x)$ comes from Eq. (15). In particular, systems involving symmetric electrolytes and relatively low surface potentials allow one to derive analytic $\psi(x)$ functions, which simplify the integrations of Eqs. (30)–(32). For slit channels, expressions of G_1, G_2 and G_3 thus obtained are presented in the Appendix A. For cylindrical channels, the respective expressions were recently reported [8] (see also [32]).

5. Application of the model: examples of illustration

This section discusses some operational situations found in analytical microfluidic devices, in order to exemplify applications of the model. Cross-shaped networks were selected for this purpose, as they are widely used for injection of samples into a given channel or fluid compartment. It may be relevant to mention first how this operation is carried out [7,10,22]: microchannels are filled with a background electrolyte solution. A sample added to the inlet of channel 1 (Fig. 3a) is transported by the solution towards channel 3, which is achieved by applying an appropriate combination of electric potentials and pressures to the ends of every channel (loading). Once the sample plug reached the intersection, potentials are conveniently switched, so that flow is established in channels 2 and 4, and simultaneously stopped in channels 1 and 3 (injection). Thus, a portion of the sample plug is taken from the intersection and conducted through the perpendicular channel. Further, to handle the size of the sample, the operation known as focusing is carried out,

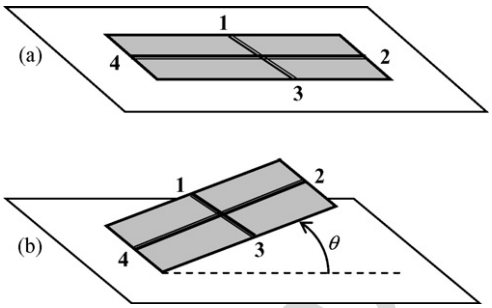

Fig. 3. Schematic representation of a cross-shaped network of microchannels: (a) placed in the horizontal plane (Cases I, II, IV and V; Table 1); (b) tilted a certain angle θ in relation to the horizontal plane (Case III; Table 1).

which basically consists in controlling the ratio $Q_{2,4}/Q_1$ during the loading step, by modifying the applied electric potentials [43].

Examples below consider EOF of symmetric electrolyte solutions, at moderate ionic concentrations, in networks of slit microchannels with $l \gg w \gg d$ (Fig. 2a) and relatively low surface potentials. Under these constraints, the geometrical factors given in the appendix ((A.3)–(A.5)) may be used in Eqs. (27)–(29) to determine the coupling coefficients. Numerical values used in calculations were arbitrarily chosen for the purpose of illustration.

5.1. Example 1: pressure effects in cross-shaped networks

As mentioned in Section 1, even when there are no applied pressures and reservoirs are open to atmosphere, pressure differences among channel ends usually arise. In relation to this, hypothetical cases related to sample injection in systems driven by EOF are discussed here. In all cases, the solution is conducted from channel 1 to channel 3 (Fig. 3a) and, for the sake of simplicity, $Q_2 = Q_4 = 0$ is imposed as a focusing condition. This should be attained, in principle, with the potential and pressure distributions reported in Table 1, Case I.

In the same table, Case II considers an excess pressure of 150 Pa in reservoir 2. A situation like this has been observed experimentally and attributed to Laplace pressures [21,22].

Table 1
Electric potential and pressure configurations in a cross-shaped network of slit microchannels

Case	ζ_3/ζ_1	P_1, V_1	P_2, V_2	P_3, V_3	P_4, V_4	P_c, V_c
I	1	0, 1000	0, 500	0, 0	0, 500	0, 500
II	1	0, 1000	150, 474.4	0, 0	0, 500	37.5, 493.6
III	1	75, 1000	0, 512.8	75, 0	150, 487.2	75, 500
IV	1.8	0, 1000	0, 333.4	0, 0	0, 333.4	−486.3, 416.5
V	0.6	0, 1000	0, 611.1	0, 0	0, 611.1	324.9, 555.7

Calculations involve EOF from channel 1 to channel 3, with $Q_2 = Q_4 = 0$. Numerical values are $d = 3\,\mu$m, $w = 100\,\mu$m, and $l = 20$ mm in all branches, while $\zeta_1 = \zeta_2 = \zeta_4 = -0.025$ V. The circulating fluid is a 10^{-4} M KCl aqueous solution at 20 °C, thus $\kappa d = 98.4$. Throughout the table, pressures are given in Pa and potentials in V.

Calculations predict the diminution required in V_2 to keep $Q_{2,4} = 0$. Also in Table 1, Case III considers pressures distribution obtained, for instance, by tilting the cross-shaped network about 25°, in the way shown in Fig. 3b [21,23]. Given this situation, V_2 must be increased and V_4 must be decreased to achieve the condition $Q_{2,4} = 0$.

One of the benefits of pure EOF is that the velocity profile is flat, as long as κd is sufficiently large, which is advantageous to avoid sample dispersions in dispensing and separation processes. This is virtually accomplished in Case I. In Cases II and III, the velocity profile is not flat anymore, because a pressure difference between the junction and channel ends remains. This aspect is better illustrated in the following example.

5.2. Example 2: cross-shaped networks with heterogeneous channels

The effect of varying the ζ-potential in straight channels without intersections [8,19,20], as well as in T-junctions [13], has been discussed in previous works. Cross-shaped networks containing branches with different ζ-potentials are analyzed here. On the base of Fig. 3a, EOF from channel 1 towards channel 3 is considered, and the condition $Q_{2,4} = 0$ is set beforehand. Table 1 (Cases IV and V) shows the potential distributions required to accomplish this focusing condition, when the surface potential of channel 3 is varied in relation to that of channels 1, 2 and 4, which are fixed at –0.025 V. Results indicate that a pressure gradient is generated along the channels, with the maximum value at the surface potential discontinuity (channel intersection in this case). It is observed in Table 1 that, when ζ_3 is higher than ζ_1 (Case IV), a negative pressure arises at the junction, and hence, the potentials V_2 and V_4 must be decreased to avoid flow from channels 2 and 4 towards the intersection. The contrary happens when ζ_3 is lower than ζ_1 (Case V).

Fig. 4 shows the velocity profiles obtained in each branch under these conditions. It is clearly seen how pressure gradients, generated because of ζ-potential discontinuities, modify fluid velocity. Indeed, the flat profile associated with pure EOF (full line in Fig. 4) is only attained when branches are perfectly homogeneous in size and surface properties. An interesting observation is that, although $Q_{2,4} = 0$ in all cases, the fluid velocity is not zero in channels 2 and 4, but a flow recirculation is predicted to occur (of course, these results do not apply in the close vicinity of junctions and channel ends). This phenomenology is also observed in the cases discussed above in Example 1.

5.3. Example 3: focusing and dispensing in double-cross networks

The double-cross injection system [10,43] is considered here, as an example of microchannel networks with two intersections. Fig. 5 illustrates the typical situation in which a sample (dark gray) is conducted from channel 1 towards channel 3′. Branches 2 and 4, the so-called focusing channels, are used to control the width of the sample plug (w_s), which is carried out by regulating the focusing ratio $V_{2,4}/V_1$. The sample is assumed to be composed of neutral molecules, and transported solely by the EOF of

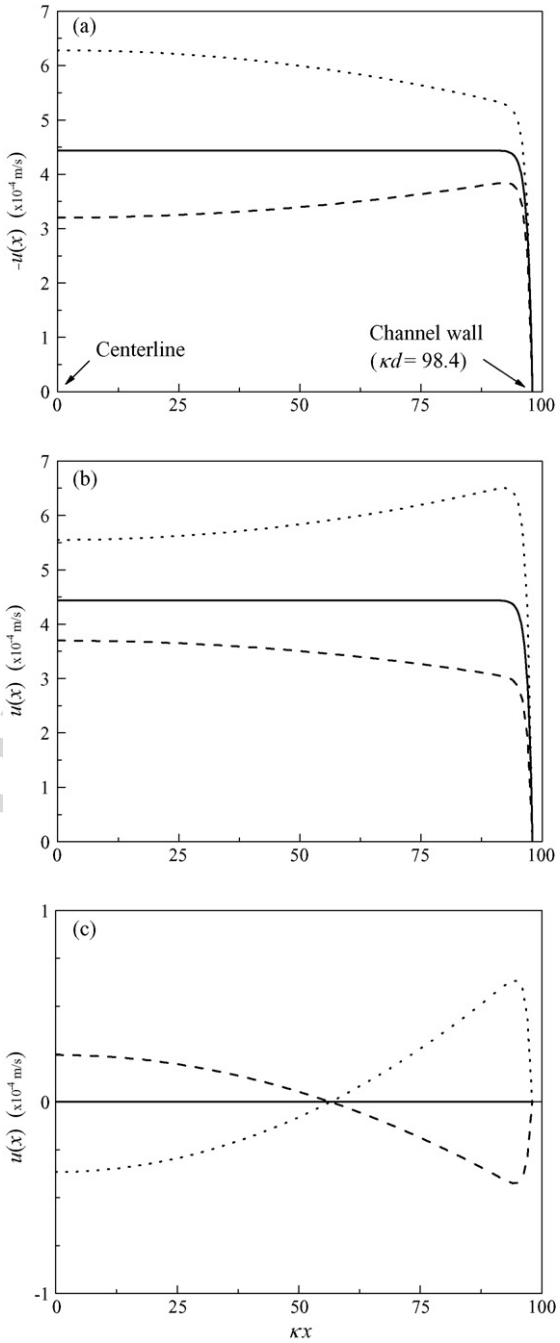

Fig. 4. Fluid velocity as a function of the relative distance κx for each branch of a cross-shaped network: (a) channel 1; (b) channel 3; (c) channels 2 and 4. Simultaneously in all branches, solid lines represent Case I ($\zeta_3/\zeta_1 = 1$), dotted lines represent Case IV ($\zeta_3/\zeta_1 = 1.8$), and dashed lines represent Case V ($\zeta_3/\zeta_1 = 0.6$). Numerical values are reported in Table 1.

the background electrolyte solution. In practical situations, this step is previous to either an electrophoretic separation through channels 2′–4′ [10], or a selective dispense of sample to one of compartments 2′, 3′ or 4′ [43].

If the sample is going to be delivered to the outlet of channel 3′, as shown in Fig. 5, appropriate values of $V_{2'}$ and $V_{4'}$ must be applied to handle the focused stream at the second junction. As a first approximation, one may impose $Q_{2'} = Q_{4'} = 0$. With this condition in the model, the required potentials $V_{2',4'}$ are calcu-

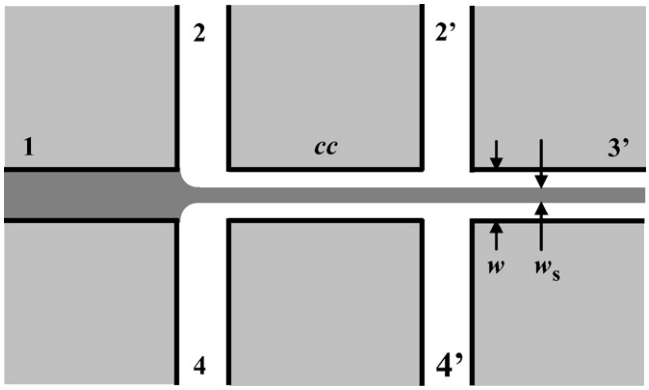

Fig. 5. Schematic representation of sample focusing carried out in a double-cross microfluidic network. Dark gray zone denotes sample, and white zone represents the background electrolyte solution. The picture intends to represent the situation where $Q_2 \approx Q_4 \approx Q_1$, hence the width of the focused sample stream is $w_s \approx w/3$, approximately, w being the channel width (see text for further details).

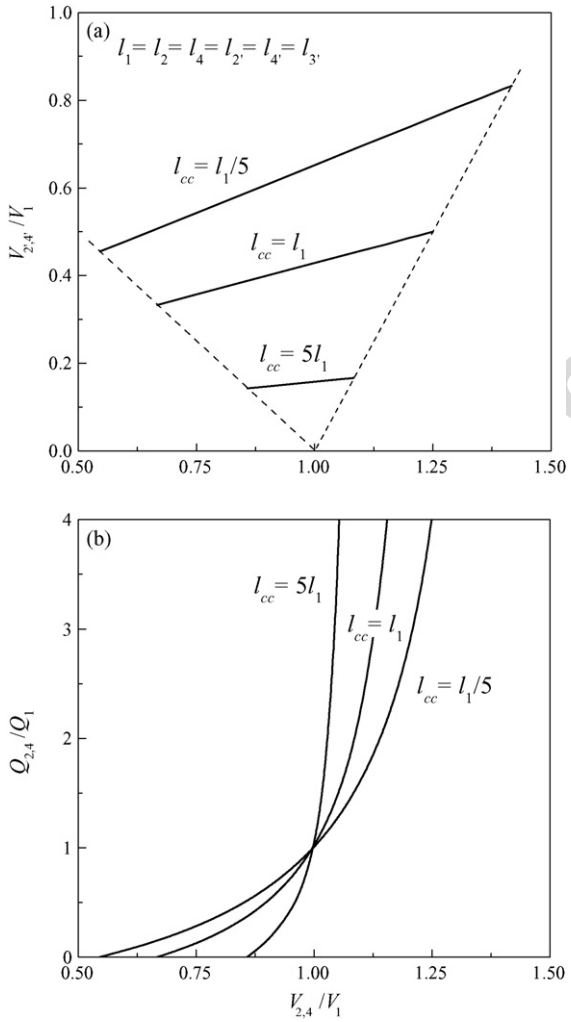

Fig. 6. (a) Relative potentials required at the ends of channels 2′ and 4′ to attain $Q_{2'} = Q_{4'} = 0$ (Fig. 5), and (b) relative flow rate in channels 2 and 4, as a function of the focusing ratio. Calculations consider a 10^{-3} M KCl aqueous solution at 20 °C ($\kappa d = 311$). Also $d = 3$ μm, $w = 100$ μm, $l = 20$ mm, and $\zeta = -0.025$ V in all branches, while $V_1 = 1000$ V and $V_{3'} = 0$. In (a), dashed lines are boundary marks for V_2 and V_4 (see related text).

lated for given values of $V_{2,4}/V_1$. Results are shown in Fig. 6a, for different lengths of common channel, while other branches are set homogeneous in size and surface properties. Dashed lines in Fig. 6a define a sort of operational window for this particular example. In fact, the lower limit of the focusing ratio is given by the potentials $V_{2,4}$ that makes $Q_{2,4} = 0$ (Fig. 6b). If one further diminishes the potentials in channels 2 and 4, the sample will leak into them from the intersection. On the other extreme, the highest values allowed for the focusing ratio are those that produce a divergence of $Q_{2,4}/Q_1$ (Fig. 6b). If one increases V_2 and V_4 beyond this limit, the sample will flow back to reservoir 1.

Finally, it is worth noting that the curves plotted in Fig. 6b offer additional features to be taken into account in the control and optimization of focusing processes. In fact, the width of the focused stream has been reported to be $w_s \approx w/(1 + 2Q_{2,4}/Q_1)$, provided a fully developed, pure EOF is attained in the network [43]. Therefore, by using data in Fig. 6b, the size of the sample stream may be directly related to the focusing ratio $V_{2,4}/V_1$. This last possibility illustrates the scope of the theoretical treatment presented in this work.

6. Concluding remarks

The present paper discusses a general procedure to deal with electrokinetic flow in microchannel networks. Calculations allow one to obtain the flow rate and the electric current in each branch of the network, for a given configuration of potential and pressure gradients. The modelling is said to be *generalized* because of the following reasons: (i) networks with multiple junctions are taken into consideration, (ii) the characteristics of every branch are included (microchannel and circulating fluid), (iii) the simultaneous presence of electric fields and pressure gradients is evaluated, (iv) both slit and cylindrical microchannels are considered in a common fashion, and (v) equations are not limited to asymptotic values of ζ-potential or Debye length. Thus, the modelling comprises microfluidic systems containing micro- and nano-scale channels, with arbitrary values of surface potential and ionic concentrations.

Examples in the last section illustrate how the theoretical approach accounts for practical situations found in analytical microsystems. Indeed, relatively simple but precise calculations may certainly help to improve the handling of these operations. Furthermore, although several improvements could be made, the modelling suggested provides an accurate basis to study more fundamental aspects of electrokinetic phenomena in microfluidics: the effect of different variables like ion conductivity, pH and surface potential, as well as the analysis of concentration profiles, can be investigated in this framework.

Acknowledgements

The author wishes to thank the financial aid received from SEPCYT-FONCyT and CONICET, Argentina.

Appendix A

Analytic expressions of the geometrical factors G_1, G_2 and G_3 can be derived for slit microchannels with relatively low surface potentials. In fact, considering symmetric electrolytes ($z_+ = -z_- \equiv z$) and large values of κd ($n_{0,+} = n_{0,-}$ and hence $\psi_0 = 0$), Eq. (15) with $m = 0$ leads to the following expression:

$$\frac{\partial^2 \Psi}{\partial x^2} = \kappa^2 \sinh(\Psi), \tag{A.1}$$

where $\Psi = ze\psi/k_B T$ is the dimensionless potential [35]. Linearizing the RHS of Eq. (A.1) about $\Psi \approx 0$ and then integrating yields,

$$\Psi(x) = Z\frac{\cosh(\kappa x)}{\cosh(\kappa d)}, \tag{A.2}$$

where $Z = e\zeta/k_B T$ (dimensionless electrokinetic potential), since boundary conditions (16) and (17) are used, with $\zeta = \psi_d$. Eq. (A.2) allows one to perform the integrations of Eqs. (30) and (31), to obtain analytic expressions of G_1 and G_2 as follows:

$$G_1 = 1 - \frac{\tanh(\kappa d)}{\kappa d}, \tag{A.3}$$

$$G_2 = \frac{\kappa d}{\cosh^2(\kappa d)}\left(\frac{\sinh(2\kappa d)}{4} - \frac{\kappa d}{2}\right). \tag{A.4}$$

In the case of G_3, after including $z_+ = -z_- \equiv z$ and $n_{0,+} = n_{0,-}$ in Eq. (32), the fraction of summations under the integral sign results $\cosh(\Psi) + \gamma \sinh(\Psi)$, where $\gamma = (\nu_+ - \nu_-)/(\nu_+ + \nu_-)$ is a factor involving the ionic mobilities. Thus, linearizing about $\Psi \approx 0$ and integrating yields,

$$G_3 = 1 + \gamma Z\frac{\tanh(\kappa d)}{\kappa d}. \tag{A.5}$$

It is worth adding here that ν_+ and ν_- are usually considered to be equal in practice, which means $\gamma = 0$ in Eq. (A.5). Nevertheless, differences in the ionic mobilities may produce significant alteration in the flow current [30].

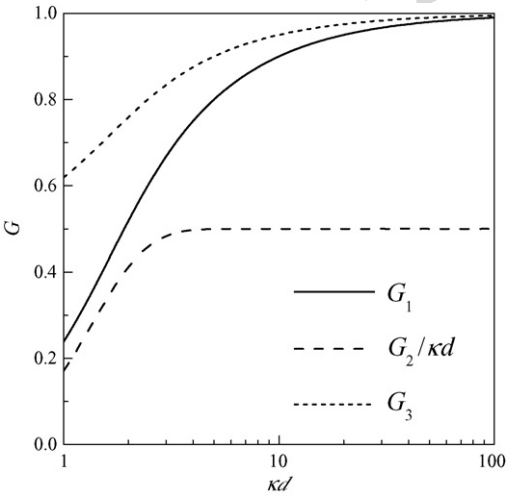

Fig. A1. Geometrical factors G_1, G_2, and G_3 for slit microchannels, as a function of the relative cross-sectional size κd, according to Eqs. (A.3), (A.4) and (A.5), respectively. In particular, $\gamma Z = -1/2$ was arbitrarily set in (A.5) for the purpose of illustration.

Fig. A1 shows the variation of geometrical factors with κd. It is observed that, when κd approaches 100, $G_1 \to 1$, $G_2 \to \kappa d/2$ and $G_3 \to 1$. These asymptotic values apply for relatively concentrated solutions ($\sim 10^{-2}$ M) in micro-scale channels, where values of κd higher than 100 are attained. Nevertheless, at low ionic concentrations ($\sim 10^{-4}$ M), or in nano-scale channels, the full expressions (A.3)–(A.5) must be used. On the other hand, the linearization of Eq. (A.1) is valid for $|\zeta| \leq 0.05$ V, approximately, as it can be deduced from the analysis of EDL potentials associated with flat interfaces [35]. Therefore, using the geometrical factors outlined in this appendix is restricted to electrokinetic flow in slit channels with relatively low ζ-potentials. The general case involves Eqs. (27)–(32), with $\psi(x)$ from Eq. (15).

References

[1] M. Freemantle, Downsizing chemistry, Chem. Eng. News 77 (1999) 27–36.
[2] J. Knight, Honey, I shrunk the lab, Nature 418 (2002) 474–475.
[3] G.M. Whitesides, A.D. Stroock, Flexible methods for microfluidics, Phys. Today 54 (2002) 42–48.
[4] D. Erickson, D. Li, Integrated microfluidic devices, Anal. Chim. Acta 507 (2004) 11–26.
[5] D.R. Walt, Miniature analytical methods for medical diagnosis, Science 308 (2005) 217–219.
[6] R.-L. Chien, L. Bousse, Electroosmotic pumping in microchips with non-homogeneous distribution of electrolytes, Electrophoresis 23 (2002) 1862–1869.
[7] S.V. Ermakov, S.C. Jacobson, J.M. Ramsey, Computer simulations of electrokinetic injection techniques in microfluidic devices, Anal. Chem. 72 (2000) 3512–3517.
[8] X. Xuan, D. Li, Analysis of electrokinetic flow in microfluidic networks, J. Micromech. Microeng. 14 (2004) 290–298.
[9] J.M. MacInnes, X. Du, R.W.K. Allen, Prediction of electrokinetic and pressure flow in a microchannel T-junction, Phys. Fluids 15 (2003) 1992–2006.
[10] L.-M. Fu, R.-J. Yang, G.-B. Lee, Electrokinetic focusing injection methods on microfluidic devices, Anal. Chem. 75 (2003) 1905–1910.
[11] E.J. van der Wouden, T. Heuser, D.C. Hermes, R.E. Oosterbroek, J.G.E. Gardeniers, A. van den Berg, Field-effect control of electro-osmotic flow in microfluidic networks, Colloids Surf. A: Physicochem. Eng. Aspects 267 (2005) 110–116.
[12] D. Li, Electrokinetics in Microfluidics, Elsevier, London, 2004.
[13] F. Bianchi, R. Ferrigno, H.H. Girault, Finite element simulation of an electroosmotic-driven flow division at a T-junction of microscale dimensions, Anal. Chem. 72 (2000) 1987–1993.
[14] D. Erickson, Towards numerical prototyping of labs-on-chip: modeling for integrated microfluidic devices, Microfluid Nanofluid 1 (2005) 301–318.
[15] H.A. Stone, A.D. Stroock, A. Adjari, Engineering flows in small devices: microfluidics toward lab-on-a-chip, Annu. Rev. Fluid Mech. 36 (2004) 381–411.
[16] R. Qiao, N.R. Aluru, A compact model for electroosmotic flow in microfluidic devices, J. Micromech. Microeng. 12 (2002) 625–635.
[17] A.N. Chatterjee, N.R. Aluru, Combined circuit/device modeling and simulation of integrated microfluidic systems, J. Microelectromech. Syst. 14 (2005) 81–95.
[18] D. Li, Electro-viscous effects on pressure-driven liquid flow in microchannels, Colloids Surf. A: Physicochem. Eng. Aspects 195 (2001) 35–57.
[19] A.E. Herr, J.I. Molho, J.G. Santiago, M.G. Mungal, T.W. Kenny, Electroosmotic capillary flow with nonuniform zeta potential, Anal. Chem. 72 (2000) 1053–1057.
[20] J.S.H. Lee, C.L. Ren, D. Li, Effects of surface heterogeneity on flow circulation in electroosmotic flow in microchannels, Anal. Chem. Acta 530 (2005) 273–282.

[21] H.J. Crabtree, E.C.S. Cheong, D.A. Tilroe, C.J. Backhouse, Microchip injection and separation anomalies due to pressure effects, Anal. Chem. 73 (2001) 4079–4086.
[22] D. Sinton, L. Ren, D. Li, Visualization and numerical modeling of microfluidic on-chip injection processes, J. Colloids Interface Sci. 260 (2003) 431–439.
[23] D. Sinton, D. Li, Electroosmotic velocity profiles in microchannels, Colloids Surf. A: Physicochem. Eng. Aspects 222 (2003) 273–783.
[24] T.T. Razunguzwa, J. Lenke, A.T. Timperman, An electrokinetic/hydrodynamic flow microfluidic CE-ESI-MS interface utilizing a hydrodynamic flow restrictor for delivery of samples under low EOF conditions, Lab Chip 5 (2005) 851–855.
[25] S.R. De Groot, Thermodynamics of Irreversible Processes, North-Holland Publishing Company, Amsterdam, 1951.
[26] R.P. Rastogi, R.C. Srivastava, S.N. Singh, Nonequilibrium thermodynamics of electrokinetic phenomena, Chem. Rev. 93 (1993) 1945–1990.
[27] E. Brunet, A. Adjari, Generalized Onsager relations for electrokinetic effects in anisotropic and heterogeneous geometries, Phys. Rev. E 69 (2004) 016306.
[28] A. Szymczyk, B. Aoubiza, P. Fievet, J. Pagetti, Electrokinetic phenomena in homogeneous cylindrical pores, J. Colloid Interface Sci. 216 (1999) 285–296.
[29] D. Burgreen, F.R. Nakache, Electrokinetic flow in ultrafine capillary slits, J. Phys. Chem. 68 (1964) 1084–1091.
[30] D. Hildreth, Electrokinetic flow in fine capillary channels, J. Phys. Chem. 74 (1970) 2006–2015.
[31] C.-H. Chen, J.G. Santiago, A planar electroosmotic micropump, J. Microelectromech. Syst. 11 (2002) 672–683.
[32] C.L. Rice, R. Whitehead, Electrokinetic flow in a narrow cylindrical capillary, J. Phys. Chem. 69 (1965) 4017–4024.
[33] F.A. Morrison Jr., J.F. Oesterle, Electrokinetic energy conversion in ultrafine capillaries, J. Chem. Phys. 43 (1965) 2111–2115.
[34] R.F. Probstein, Physicochemical Hydrodynamics, Butterworths, New York, 1989.
[35] R.J. Hunter, Foundations of Colloid Science, vols. I and II, Clarendon Press, Oxford, 1992.
[36] X. Xuan, D. Li, Electroosmotic flow in microchannels with arbitrary geometry and arbitrary distribution of wall charge, J. Colloid Interface Sci. 289 (2005) 291–303.
[37] T. Zhou, A.-L. Liu, F.-Y. He, X.-H. Xia, Time-dependent starting profile of velocity upon application of external electrical potential in electroosmotic driven microchannels, Colloids Surf. A: Physicochem. Eng. Aspects 277 (2006) 136–144.
[38] T.W. Healy, L.R. White, Ionizable surface group models of aqueous interfaces, Adv. Colloid Interface Sci. 9 (1978) 303–345.
[39] A.V. Delgado, F. González-Caballero, R.J. Hunter, L.K. Koopal, J. Lyklema, Measurement and interpretation of electrokinetic phenomena (IUPAC Technical Report), Pure Appl. Chem. 77 (2005) 1753–1805.
[40] C.L.A. Berli, M.V. Piaggio, J.A. Deiber, Modeling the zeta potential of silica capillaries in relation to the background electrolyte composition, Electrophoresis 24 (2003) 1587–1595.
[41] C.L.A. Berli, M.V. Piaggio, J.A. Deiber, Theoretical relation between the tube zeta potential and the background electrolyte composition in capillary electrophoresis, Prog. Colloids Polym. Sci. 128 (2004) 21–24.
[42] S.S. Dukhin, R. Zimmermann, C. Werner, A concept for the generalization of the standard electrokinetic model, Colloids Surf. A: Physicochem. Eng. Aspects 195 (2001) 103–112.
[43] R.-J. Yang, C.-C. Chang, S.-B. Huang, G.-B. Lee, A new focusing model and switching approach for electrokinetic flow inside microchannels, J. Micromech. Microeng. 15 (2005) 2141–2148.